ISSN 1349-1113
JAXA-RR-14-012E

JAXA Research and Development Report

Results on International Collaboration of Complex Plasmas in Microgravity and on Earth by Use of PK-3 Plus Facility

JAXA PK-3 Plus Mission Team

March 2015

Japan Aerospace Exploration Agency

ISSN 1349-1113
JAXA-RR-14-012E

JAXA Research and Development Report

Results on International Collaboration of Complex Plasmas in Microgravity and on Earth by Use of PK-3 Plus Facility

JAXA PK-3 Plus Mission Team

March 2015

Japan Aerospace Exploration Agency

PREFACE

This is the final report of the first international collaboration of the complex plasmas experiments in microgravity by use of the second-generation apparatus on the International Space Station (ISS), PK-3 Plus (Plasmakristall-3 Plus). PK-3 Plus was developed by the science team at the Max-Planck Institute for Extraterrestrial Physics (MPE). After development was completed, PK-3 Plus was transferred to the Joint Institute for High Temperatures (JIHT, previously called Institute for High Energy Densities) of the Russian Academy of Sciences (RAS). JIHT, Roscosmos (Russian Federal Space Agency), and Energia jointly launched PK-3 Plus by a Russian Progress cargo spacecraft in December 2005. The first experiment was carried out in January 2006 and the operation was terminated in June 2013. The PK-3 Plus has similar configurations to the first apparatus PKE Nefedov, that is, two RF electrodes surrounded by the grounded rings. However, the size of grounded ring was changed so that so-called a void region could be suppressed as much as possible. The void region is the region without any particles.

Prof. Dr. Totsuji, who is the principal investigator of the Japanese team, established an important theory about the critical phenomena of charged systems in 1974. He thought that the critical phenomena of charged systems might be observed since the particle charge in the complex plasmas should be much larger than the ions and electrons charges. This new idea was proposed to the PK-3 Plus science team at the meeting on the critical phenomena, which was held in May 2006 in Orléans, France. This was the beginning of the international collaboration.

After the advance in collaboration, we started a microgravity-experiment mission at the ISS Science Project Office of the Japan Aerospace Exploration Agency (JAXA) in January 2007. This mission was authorized by the science committee for the space environment utilization at the Institute of Space and Astronautical Science (ISAS), JAXA, which is an advisory committee to the director general of the ISAS. The authorization process was triggered by a letter from Prof. Dr. Dr.h.c. G. E. Morfill who is the principal investigator at the MPE. The microgarvity necessity, scientific significance, research plan, cost and team members were reviewed by the committee.

In December 2007, we got the first trial of microgravity experiment. The experimental condition was based on the theoretical work by Prof. Dr. Totsuji. Unfortunately, the total number of particles was not large since the observable area was decreased due to a large void region. Since then, the suppression of the void region was become as one of the most important issues for us.

From December 2007 to June 2013, we fortunately joined seven missions. We did not expect many chances of the microgravity experiments at the beginning of the JAXA mission. We are deeply grateful to all of the international team members for giving us the invaluable chances. We have been analyzing the data to know how close we approach to the critical point. Unfortunately, the preliminary results show the critical point is not so close. To reach the critical point, we may need more power. More power means a larger void region. Therefore, the void suppression technology will be required in the higher power experiments.

The unique theoretical and experimental researches have been carried out by the Japanese team. From the theoretical point of view, the original theory of the critical phenomena is the most important. The theory does not require the Lennard-Jones potential. Other theoretical works related to experimental data analysis is also excellent. To know how close to the critical point, these researches are indispensable. On the other hand, from the experimental point of view, the probe measurements bring us important results. Since PK-3 Plus has no diagnostics except for the video camera, the probe measurement on the ground is one of the key data to analyze the experimental data in microgravity. Data analysis has been continuing. It will take more time until complete the analysis. There are many valuable data. However, more than 1 year is past from the last international science meeting in Moscow. Therefore, we summarize and conclude our results as the termination of the Japanese team for PK-3 Plus.

The period of the PK-3 Plus collaboration is more than 8 years from January 2007 to March 2015. This may be the longest duration for the microgravity experiment in Japan. I would like to sincerely thank the team members for the long and important mission. And I also wish to work together in near future, hopefully the next international collaboration of PK-4.

JAXA PK-3 Plus Mission Team
Team Coordinator
Satoshi Adachi

Contents

Collaborative Experiments of PK-3 Plus in Space

Satoshi ADACHI [*1, *2], Kazuo TAKAHASHI [*3], and Hiroo TOTSUJI [*4]

Abstract: Microgravity experiments of complex plasmas were carried out through the international collaboration on the International Space Station (ISS). The apparatus is named PK-3 Plus, which is the second-generation apparatus on the ISS. Due to the limitation of weight and size, cameras with four different fields of view are the main diagnostics of PK-3 Plus. Therefore, indispensable parameters to understand behavior of the complex plasmas are estimated from measurements on the ground and calculations. In this paper, several important parameters for the critical phenomena of charged systems are estimated.

Keywords: Complex Plasmas, PK-3 Plus, Microgravity, ISS

1. Introduction

Complex plasmas contain electrons, ions, and particles. This type of plasma is observed in the universe, for example, nebulae, proto-planetary disks, and interstellar molecular clouds. The complex plasmas have a unique feature that strongly coupled plasma is easily achieved. In 1986, it was theoretically predicted that sufficiently strong coupling made the particles ordered structure [1]. The ordered structure is called a plasma crystal or Coulomb crystal nowadays. This was a good trigger of new research on the Coulomb crystal in laboratories. In 1994, several researchers successfully observed the Coulomb crystal formation in their laboratories [2–5]. The particles, however, must be levitated from electrodes against the gravity to form the Coulomb crystal on the ground so that they could move freely. This means that the particles are located in the sheath region formed near electrodes. This causes two major problems, that is, one is the particles exist in the non-plasma region, and the other is the structure of the Coulomb crystal is deformed by the ion flow. These problems drastically increase the difficulty of researches on critical phenomena, predicted phase diagrams, equilibrium crystal shapes, crystal formation mechanisms, and so on. This is the main reason why the microgravity is required.

The first apparatus installed on the International Space Station (ISS) was PKE-Nefedov [6–8], which had been operated from March 2001 to July 2005. In the microgravity experiments, a large area in which the particles do not exist was formed. Today this particle-free region is simply called the void. Although the void influence on the behavior of the complex plasmas is not clear yet, it is clear that the particle existence area becomes smaller. This means that the total number of particles within the observation area and the effective size of the Coulomb crystal are decreased. Therefore, the void-free plasma should be much better for the microgravity experiments.

The second apparatus named PK-3 Plus [9–12] had been operated from January 2006 to June 2013 on the ISS. This is an improved apparatus based on PKE-Nefedov to suppress the void. We had an interest in this facility to investigate the critical phenomena of the charged systems. Therefore, a new model [13–15] was proposed to the international research team. The team had a strong interest in this model. Thus multiple machine times were assigned to the critical phenomena research. One of the most important issues was to determine appropriate experimental conditions of three adjustable parameters, that is, particle size, RF power, and gas pressure. Unfortunately, PK-3 Plus has four cameras with different fields of view but does not have any other major diagnostics such as a Langmuir probe, spectrometer, microwave interferometer, and so on. This means the experimental conditions should

* Received 8 January, 2015

*1 Institute of Space and Astronautical Science, Japan Aerospace Exploration Agency, 2-1-1 Sengen, Tsukuba, Ibaraki 305-8505, Japan
*2 School of Physical Sciences, Graduate University for Advanced Studies (SOKENDAI)
*3 Department of Electronics, Kyoto Institute of Technology, Matsugasaki, Sakyo-ku, Kyoto 606-8585, Japan
*4 Okayama University, 3-1-1 Tsushimanaka, Kitaku, Okayama 700-8530, Japan
(E-mail: adachi.satoshi@jaxa.jp)

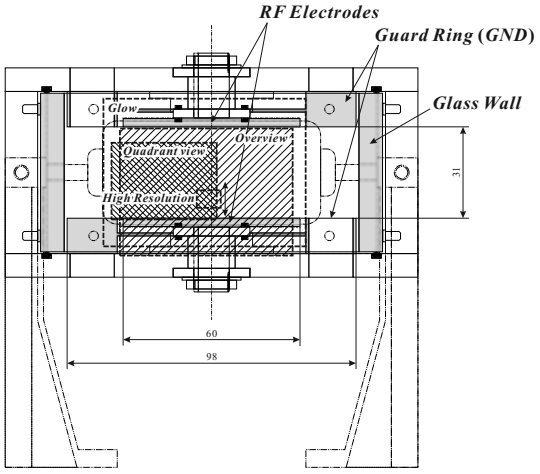

Fig. 1 Schematic view of PK-3 Plus.
Two RF electrodes of 60 mm in diameter, which are surrounded by grounded rings of 98 mm in outer diameter, are set. The distance between the electrodes is 31 mm.

be determined by quantitative estimation based on results of measurements on the ground and calculations. Therefore, we calculate the required parameters such as the charges and Coulomb coupling parameter.

2. PK-3 Plus

The apparatus PK-3 Plus basically has similar structure to PKE-Nefedov, that is, two RF electrodes surrounded by grounded rings. However, the electrodes and grounded rings are bigger than those of PKE-Nefedov so that the void could be suppressed. The schematic view of PK-3 Plus is shown in Fig. 1. Six particle dispensers are installed. The particle sizes are 1.5, 2.5, 3.4, 6.8, 9.2, and 14.9 μm in diameter. The maximum output power from the RF oscillator is 4 W. PK-3 Plus has four cameras with difference fields of view as the main diagnostics. The cameras are called the glow, overview, quadrant view, and high resolution cameras, corresponding to the sizes of fields of view. Each field of view is also indicated in Fig. 1. The glow camera has a optical filter to observe luminescence from excited atoms or ions.

Our objective is to approach the critical point as closer as possible as mentioned above. The theory predicts that the larger particle should be more suitable for the observation of critical phenomena. The large particle, however, makes the void size larger. The large void means the total number of particles and the size of observation area are decreased. As a result, the reliability of structure factor and pair correlation is deteriorated, especially at the long distance. Therefore, experimental conditions that can be reduce the void size as much as possible are required.

The theory also predicts necessary plasma parameters for the critical point. Since PK-3 Plus does not have the diagnostics of plasma parameters such as density and temperature, some parameters are assumed to be the same as those measured on the ground. Other parameters are estimated by calculation and the measurements on the earth. By using these parameters, the experimental conditions are determined.

3. Parameter Estimation Method

There are several parameters indicating the status of the complex plasmas. The important ones are the Coulomb coupling parameter Γ, inter-particle mean distance a, electron and ion densities, n_e and n_i, electron and ion temperatures, T_e and T_i, number density of particles n_d, particle temperature T_d, and particle charges Q_d. The Coulomb coupling parameter Γ is defined as the ratio of the Coulomb energy to the kinetic energy, that is,

$$\Gamma = \frac{{Q_d}^2}{4\pi\varepsilon_0 a k_B T_d} . \quad (1)$$

The electron and ion densities and electron temperature can be measured by a single or double probe in principle. Unfortunately, PK-3 Plus does not have any probes. Prof. Takahashi has been investigating the density profiles in PK-3 Plus on the ground [16]. The influence of thermal convection of the neutral gas on the density and temperature profiles may be negligibly small. Therefore, it is assumed that these profiles in space are similar to those on the ground.

The ion temperature is difficult to be measured and thus it is usually assumed to be the same as the room temperature. This assumption is reasonable since the number density of neutral atoms is more than 10^6 times higher than the ion density in many cases and thus the ions rapidly lose the kinetic energy by the Coulomb collision with the atoms. The particle temperature is also often assumed to be the room temperature, but the particle energy is not easily reduced by the collision with the neutral atoms as compared with the ion energy due to the much heavier mass than the ion mass. In this paper, the particle temperature is obtained from

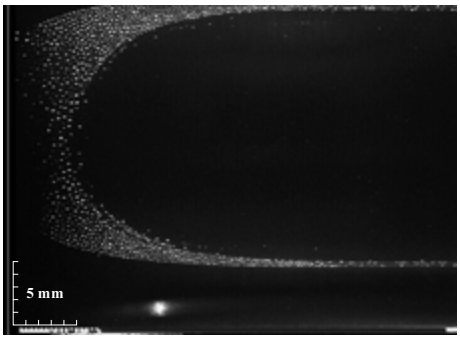

Fig. 2 Typical experimental results in space. The pressure and RF power are set to 20 Pa and 1.8 W, respectively.

the velocity distribution function (VDF). The VDF is obtained from the data analysis of video data.

The distance between the nearest neighbor particles, d is obtained from the pair distribution function (PDF). The PDF is also obtained from the video data. The charge is estimated by considering the following conditions;

$$Q_d = 4\pi\varepsilon_0 r_d \Delta\phi \,, \tag{2}$$

$$-en_e + Q_d n_d + Zen_i = 0 \,, \tag{3}$$

$$j_e + j_i = 0 \,, \tag{4}$$

where r_d, Z, j_e, and j_i represent the particle radius, charge number of ions, electron and ion current densities, respectively. $\Delta\phi$ is defined as $\phi_d - \phi_p$, where ϕ_d and ϕ_p represent the potential on the particle surface and plasma potential, respectively. The electron and ion current densities are described as

$$j_e = -en_{e0}\sqrt{\frac{k_B T_e}{2\pi m_e}} \exp\left\{\frac{e(\phi-\phi_p)}{k_B T_e}\right\} \,, \tag{5}$$

$$j_i = Zen_{i0}\sqrt{\frac{k_B T_i}{2\pi m_i}} \exp\left\{1 - \frac{Ze(\phi-\phi_p)}{k_B T_i}\right\} \,. \tag{6}$$

The ion current density is came from the orbital motion limited theory. By combing those equations, the final equation is obtained as follows;

$$-Zen_i\sqrt{\frac{T_i}{T_e}}\sqrt{\frac{m_e}{m_i}}\left(1-\frac{e\Delta\phi}{k_B T_i}\right)\exp\left(-\frac{e\Delta\phi}{k_B T_e}\right) + 4\pi\varepsilon_0 r_d n_d \Delta\phi + Zen_i = 0 \,. \tag{7}$$

In weakly ionized plasma like complex plasmas, the charge number Z is usually 1.

The other important parameters related to the critical point are defined as follows;

$$\xi = \frac{a}{\lambda_D} \,, \tag{8}$$

$$A = \frac{n_e k_B T_e + n_i k_B T_i}{n_d k_B T_d} \,, \tag{9}$$

$$\Gamma_0 = \frac{{Q_d}^2}{4\pi\varepsilon_0 r_d k_B T_d} = \Gamma\frac{a}{r_d} \,, \tag{10}$$

where λ_D represents the Debye length. Although these are not the independent parameters but are calculated from other parameters, these are convenient to understand how close to the critical point.

4. Results and Discussion

The parameters required for the critical point are theoretically predicted. One example of the parameter set is shown in Table 1. These parameters must be translated to operation parameters, that is, the particle size, pressure, RF power.

It is clear from Eq. (2) that the larger particle size is more suitable for obtaining larger particle charge,

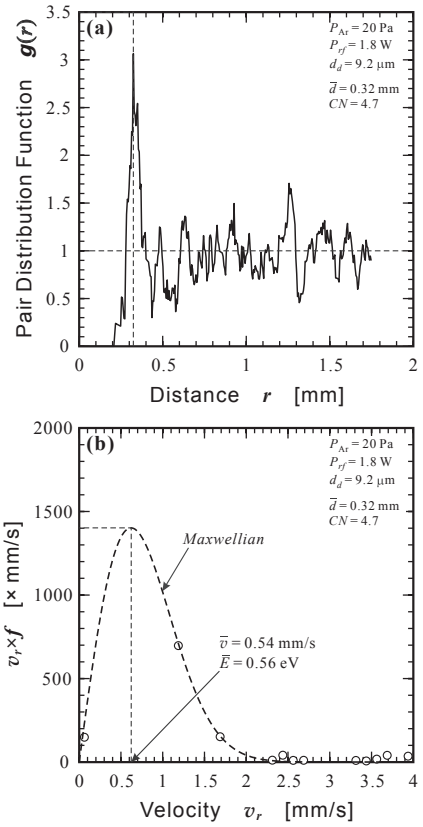

Fig. 3 (a) Pair distribution function and (b) velocity distribution function. These functions are obtained from the data shown in Fig. 2.

Table 1 Theoretically obtained parameters for the critical point.
T_d is assumed to be the same as T_i.

ξ	4
T_i [eV]	0.03
T_e [eV]	3
n_i [cm^{-3}]	10^9
n_e [cm^{-3}]	10^7
n_d [cm^{-3}]	5×10^5
A	10^4
Γ	2×10^4
Γ_0	2×10^5

Table 2 Experimentally obtained parameters representing the status of complex plasmas.
T_i is assumed to be 0.03 eV.

ξ	2.0
T_e [eV]	1.2
n_i [cm^{-3}]	1.6×10^8
n_e [cm^{-3}]	0.2×10^8
n_d [cm^{-3}]	2.8×10^4
A	8500
Γ	320
Γ_0	1.4×10^4
Q_d	$5000e$

which makes the Coulomb coupling stronger. On the other hand, it seems that the larger particle makes the void region size larger. In addition, the higher power is required to obtain the higher density, though the higher power also makes the void region size larger. The research on the critical phenomena needs the observation area as large as possible since the long-range correlation is important to know how close to the critical point. Therefore, the void formation must be suppressed as much as possible. These are the conflicting requirements. Therefore, the prioritization of experimental conditions is indispensable.

We focused on the particle charge first because it is impossible to approach the critical point if the charge is small. From this point of view, the largest particle of 14.9 μm is the best choice but the void will be the largest. Therefore, we select the second largest particle, 9.2 μm in diameter to reduce the void size. The typical experimental result in space is shown in Fig. 2. The bright points are the 9.2 μm-particles. It is found that the large void region is formed. By detecting the particles and obtaining the coordinates of particles, the PDF is obtained. The VDF is also obtained by tracing the time evolution of the particle coordinates. These are shown in Fig. 3. From Fig. 3(a), it is found that d is obtained from the distance at the first peak and is 0.32 mm. The coordination number, which indicates the number of particles surrounding one particle, is 4.7 in this case. By considering that the ideal coordination number is 6 in the case of two-dimensional Coulomb crystal, this number suggests that the Coulomb crystal was not clearly formed or was much deformed. In Fig. 3(b), the curved dashed-line represents the best-fitted two-dimensional Maxwellian. By comparing the experimental data with the Maxwellian, it is found that the average velocity of particle is 0.54 mm/s and thus the particle temperature is 0.56 eV. The temperature is almost 20 times higher than the room temperature. This may increase the difficulty in observing the critical phenomena.

The inter-particle mean distance, or the Wigner-Seitz radius, a is calculated from d to be 0.205 mm. To obtain the three-dimensional parameters from the two-dimensional data, the conversion factor[17] must be taken in account. Once the parameter a is obtained, the number density of particle is calculated to be 2.8×10^4 cm^{-3}. The electron and ion densities are almost the same at the location being far enough from the Coulomb crystal and are 1.6×10^8 cm^{-3} from the probe measurement on the ground. The electron temperature is also measured by the probe and is about 1.2 eV in this case. The ion temperature is assumed to be 0.03 eV as mentioned previously. Thus Eq. (7) can be solved by substituting these values into the equation. The potential difference $\Delta\phi$ is obtained to be -1.58 V. Thus the charge is estimated to be about $5000e$. The other parameters are also calculated and are summarized in Table 2.

By comparing Table 2 with Table 1, it is found that the ion density is too low. This suggests the RF power is low. The low electron temperature supports this suggestion. The parameters ξ and A are not bad, while Γ is too small. Although the Γ value of 320 is larger than the lower limit of the three-dimensional crystallization, i.e., 178, this value is not large enough to ob-

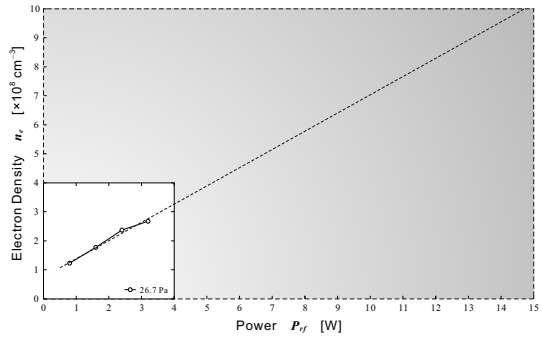

Fig. 4 Required power estimated by extrapolating the density dependence on the power.

tain good long-range order. This is qualitatively consistent with the PDF indicating no good long-range order. To increase the Γ value, the higher power should also be suitable. These results indicate that the current condition of complex plasma is not very close to the critical point.

Therefore, we investigate more appropriate operation conditions. First, we estimated the required RF power by extrapolating the density dependence on the power. The result is shown in Fig. 4. The figure shows that the power of 14 W or more is required to achieve the density of 10^9 cm^{-3} under the assumption of linear dependence. Actually, such the linear dependency is rarely obtained. Therefore, 20 W or more may be necessary, which is much higher than the power of PK-3 Plus. Preparation of such power source is not technically difficult. The large power, however, the large void is formed. As shown in Fig. 2, the observation area is small in the power of 1.8 W. If the 20 W power was supplied to PK-3 Plus, almost all particles might be disappeared. To avoid that, the void formation mechanisms must be understood more deeply.

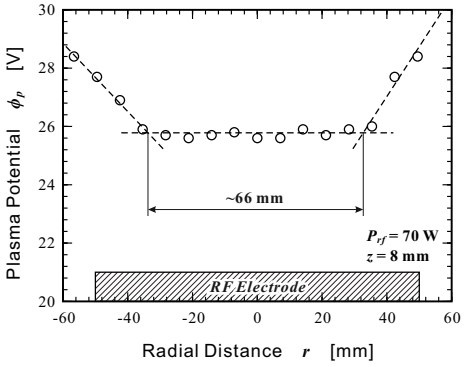

Fig. 5 Radially flat potential profile measured in the large-sized apparatus on the ground.
The electrode diameter is 100 mm, which is similar to the outer diameter of grounded ring.

However, the essential solution should be the flatter potential profile. It is difficult to achieve such the profile.

Fortunately, one of our apparatuses for the ground experiments has a radially flat potential as shown in Fig. 5. Since this apparatus has a large vacuum chamber, the wall influence on the potential should be negligibly small. The Coulomb crystal is formed within the region of flat potential on the ground-based experiments. If the particle is accidentally located at the outer place where the potential increases, the particle runs away from the electrode with acceleration caused by the electric field.

We recently start the investigation by using the smaller model. The current result is shown in Fig. 6. The helium gas of 67 Pa and particle of 2 μm in diameter are used. From the figure, it is found that the particles are filled in almost all the lower half part of apparatus without the void. However, this may not indicate the void is suppressed in space. The short-period microgravity experiments are required to investigate the void formation in this apparatus. Before planning such expensive experiments, we will investigate the characteristics of apparatus more deeply.

5. Conclusions

We joined the international research team for the complex plasmas by using the PK-3 Plus apparatus. One of the objectives was the critical phenomena. The Japanese science team proposed the experimental and operation conditions in space. The international team carried out the microgravity experiments based on our proposal multiple times. The largest and second largest particles were used in the experiments due

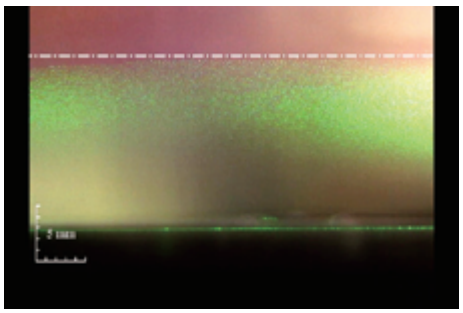

Fig. 6 Coulomb cloud observed in the small apparatus.
The horizontal dot-dashed line represents the midplane of the apparatus.

to the necessity of large charges. The high power was also supplied to the apparatus to increase the plasma density. However, these caused the formation of large void region. As a result, the observation area was much decreased.

By analyzing experimental data, it is found that the power is still small for the critical phenomena. It is estimated that the power of 15 to 20 W may be required by extrapolating the density dependence on the power. Such large power caused the large void formation. Therefore, the void suppression is required. To suppress the void, theoretical and experimental works are necessary. Recently, experimental investigation using a small-sized apparatus having similar dimension to PK-3 Plus. Although the characteristics of apparatus is not well understood yet, some results show possibility of improvement in the void formation.

Acknowledgment

The authors are deeply grateful to all members of the international science team of PK-3 Plus, DLR, ROSCOSMOS, ENERGIA, ESA and other related organization for the international collaboration.

References

1) Ikezi, H., Phys. Fluids, Vol. 29, (1986), pp. 1764–1766.
2) Thomas, H., Morfill, G. E., Demmel, V., Goree, J., Feuerbacher, B., and Möhlmann, D., Phys. Rev. Lett., Vol. 73, (1994), pp. 652–655.
3) Chu, J. H. and Lin, I., Physica A, Vol. 205, (1994), pp. 183–190.
4) Melzer, A., Trottenberg, T., and Piel, A., Phys. Lett. A, Vol. 191, (1994), pp. 301–308.
5) Hayashi, Y. and Tachibara, K., Jpn. J. Appl. Phys., Vol. 33, (1994), pp. L804–L806.
6) Morfill, G. E., Thomas, H. M., Annaratone, B. M., Ivlev, A. V., Quinn, R. A., Nefedov, A. P., Fortov, V. E. *et al.*, AIP Conf. Proc., Vol. 649, (2002), pp. 91–109.
7) Nefedov, A. P., Morfill, G. E., Fortov, V. E. *et al.*, New J. Phys., Vol. 5, (2003), pp. 33.1–33.10.
8) Fortov, V. E., Vaulina, O. S., Petrov, O. F. *et al.*, Phys. Rev. Lett., Vol. 90, (2003), 245005.
9) Thomas, H. M., Morfill, G. E., Fortov, V. E. *et al.*, New J. Phys. Vol. 10, (2008), 033036.
10) Thomas, H. M., Morfill, G. E., Ivlev, A. V. *et al.*, Multifacets Dusty Plasmas, Vol. 1041, (2008), pp. 41–44.
11) Hofmann, P., Seurig, R. Stettner, A. *et al.*, Acta Astronautica, Vol. 63, (2008), pp. 53–60.
12) Takahashi, K., Thomas, H. M., Morfill, G. E., Ivlev, A. V., Hayashi, Y., and Adachi, S., Multifacets Dusty Plasmas, Vol. 1041, (2008), pp. 329–330.
13) Totsuji, H., Phys. Plasmas, Vol. 15, (2008), 072111.
14) Totsuji, H., Plasma Fusion Res., Vol. 3, (2008), 046.
15) Totsuji, H., J. Phys. A: Math. Theor., Vol. 42, (2009), 214022.
16) Takahashi, K., Hayashi, Y., and Adachi, S., J. Appl. Phys., Vol. 110, (2011), 013307.
17) Totsuji, H., J. Phys. Soc. Jpn., Vol. 78, (2009), 065004.

Measurement of Ion Density and Electron Temperature by Double-Probe Method to Study Critical Phenomena in Dusty Plasmas

Kazuo TAKAHASHI [*1], Satoshi ADACHI [*2], and Hiroo TOTSUJI [*3]

Abstract: A dusty plasma research was performed to investigate critical phenomena in JAXA, participating in missions of a joint Russian/German Scientific project with cooperation of the PK-3 plus flight module on the International Space Station. In the research, it was necessary to obtain plasma parameters such as densities and temperatures of electron and ion for analyzing a state of dusty plasmas expressed by parameters in a phase diagram of Coulomb coupling parameter and ratio of inter-particle distance to Debye length. This work was dedicated to obtain ion density and electron temperature by using a double-probe method. The ion density was measured to be in the order of 10^8–10^9 cm^{-3}. The electron temperature was observed to be enhanced by injecting dust particles to the plasmas.

Keywords: Dusty Plasma, Fine Particle Plasma, Complex Plasma, PK-3 Plus, Microgravity, ISS

1. Introduction

This research was motivated in the experiments on the International Space Station (ISS) of dusty (complex or fine particle) plasmas, which had been going on with collaboration between Max-Planck-Institute for Extraterrestrial Physics (MPE, Germany) and Joint Institute for High Temperatures (JIHT, Russia) for several years.

Plasmas including dust particles (typically, micrometer-sized), so-called dusty plasmas, have attracted considerable scientific interest in recent decades. The dust particles are charged by fluxes of electron and ion in the plasmas. The charge of dust particles can be in the order of a few thousands of elementary charge in typical laboratory plasmas. The charged dust particles are regarded as a strongly coupled Coulomb system. In the system, one can observe many physical phenomena found in solid or liquid state, such as crystallization, phase transition, wave propagation, and so on.

Complex plasma experiments have been done in microgravity conditions with apparatuses boarding on parabolic flight, sounding rocket and the ISS for recent years. Several physical phenomena, e.g., wave propagation and so on, have been reported by MPE and JIHT in the experiments on the ISS. The utility for dusty plasmas on the ISS was replaced an improved apparatus denoted by PK-3 plus set in the Russian module at the end of 2005 [1)].

Several scientists in Japan have joined to the mission of PK-3 plus since July 2009, for demonstrating a critical phenomenon in dusty plasmas predicted in calculation by one of the authors [2)]. Plasmas of high density were required to approach to the critical point. Referring a previous work for diagnostics in PK-3 plus, high power and high pressure conditions were employed to obtain the plasmas of high density [3)]. In the previous diagnostics, electron densities were measured by the hairpin resonator, which was relatively large antenna compared with size of chamber and possibly affected the plasmas. In the present research, a double-probe method was used for measuring ion density and electron temperature to reduce disturbance in the plasmas and examined the results from the hairpin resonator.

2. Diagnostics in Dusty Plasmas

2.1 Measurement of electron density by hairpin resonator

The previous work was done for measurements of electron density with a hairpin resonator in the PK-3 plus apparatus, equipped with parallel plate electrodes

*1 Department of Electronics, Kyoto Institute of Technology, Matsugasaki, Sakyo-ku, Kyoto 606-8585, Japan
*2 Institute of Space and Astronautical Science, Japan Aerospace Exploration Agency, 2-1-1 Sengen, Tsukuba, Ibaraki 305-8505, Japan
*3 Okayama University, 3-1-1 Tsushimanaka, Kitaku, Okayama 700-8530, Japan
(E-mail: takahash@kit.jp)

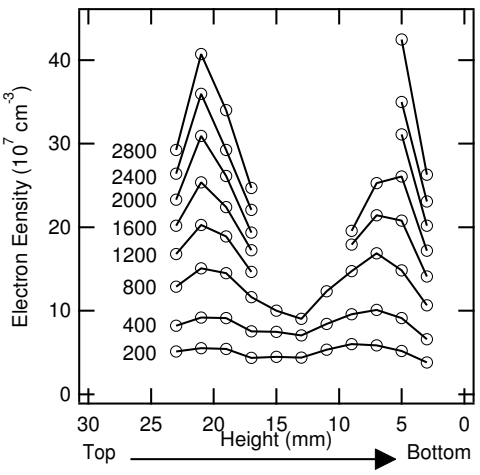

Fig. 1 The spatial distribution profiles of electron density between top and bottom electrodes at 40 Pa, measured with changing rf power from 200 to 2800 mW.

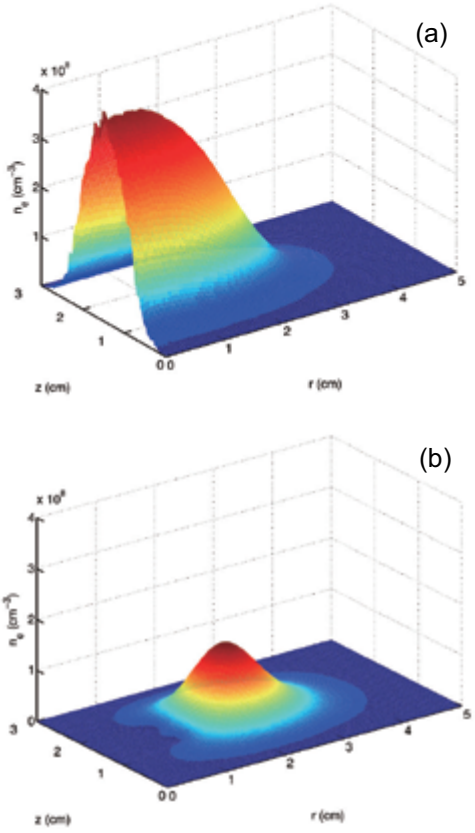

Fig. 2 The spatial distribution profiles of electron density in a Ne plasma calculated by a PIC/MCC code, (a) a pristine plasma, and (b) the plasma with the antenna of hairpin.

surrounded by grounded guard rings in a chamber[3]. The electrodes at top and bottom sides were separated 30 mm. The diameter of the electrodes was 60 mm.

Figure 1 shows spatial distribution profiles of electron density between the top and bottom electrodes in Ar plasmas at 40 Pa, measured with changing rf power from 200 to 2800 mW. Two peaks are found in the profiles of electron density at distance of 8 mm from each electrode. Conversely, the profile was simulated for a Ne plasma by a particle-in-cell Monte Carlo code (PIC/MCC)[4]. The electron density is the highest at the axial and radial center in the pristine plasma without an antenna of the hairpin resonator (Fig. 2 (a)). Introducing the hairpin resonator to the center of the chamber, electrons are missed around the hairpin resonator, and the density of electron is reduced all over the chamber (Fig. 2 (b)). The plasma is affected by the hairpin resonator and electrons are lost on its surface. Therefore it is reasonable to think that the profile of electron density obtained by the hairpin resonator misses the highest around the center of the plasma and the electron density is estimated under that of the pristine plasma.

2.2 Measurement of ion density and electron temperature by double-probe method

Hindering loss of electron on an equipment for diagnostic, a traditional double-probe method was employed, which did not take electrons and ions as currents in an electrical circuit for the method[5,6]. Ion density and electron temperature were measured with the tips of 0.35 mm in diameter, 8 mm in length and separated 7 mm each other, which were made of tungsten wire (Fig. 3).

The tips were connected to a voltage source with floating on the ground of plasmas. Figure 4 shows pictures of the tips introducing to a dust cloud illuminated by a laser. Here dust particles of 2.6 μm in diameter were injected with extremely high density, and instability and wave were excited in the dust cloud. The tips were set at 8 mm high from the bottom electrode and surrounded by the sheath, where corresponds to a dust-free region[7,8]. In the figure, the right tip is initially applied -30 V negative to the left one. The voltage was swept to +30 V with sampling current in an electrical circuit insulated from that for generating plasmas. When the tip has negative potential to the other, a sheath of corrected ions around the tip expands to thickness determined by the Bohm criterion. The dust particles reach to an equilibrium position near

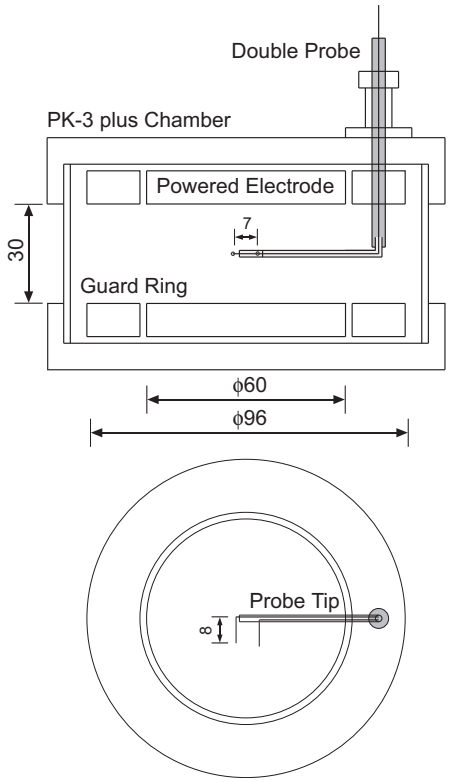

Fig. 3 Schematics of the PK-3 plus chamber and the tips for the double-probe method.

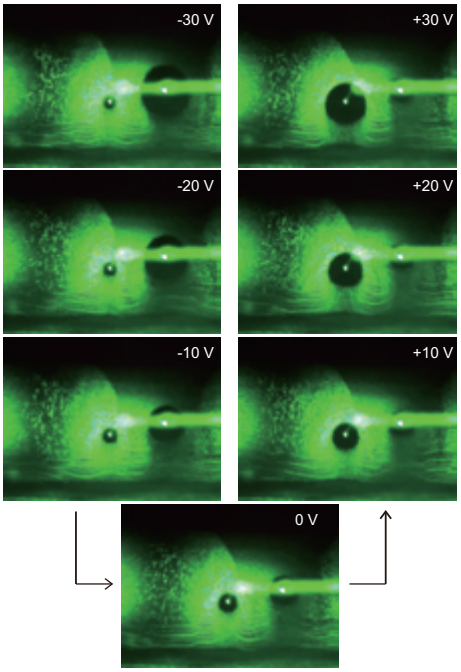

Fig. 4 Pictures of the tips for the double-probe method introduced to the dust cloud in the plasma. The tips were set at 8 mm high from the bottom electrode. The dust particles were illuminated by a laser and observed to distribute from 2.5 to 13 mm high. The right tip was negatively biased at -30 V to the left one, initially. The bias voltage was changed to positive side and reached to +30 V.

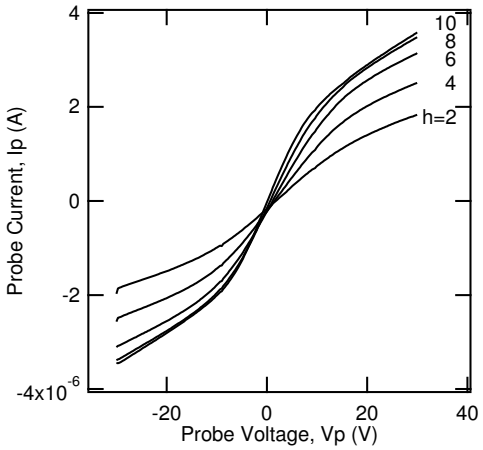

Fig. 5 Electric characteristics in the double-probe method. The probe currents (I_p) were plotted as functions of voltage applied between the tips (V_p). The curves were obtained with changing height of the tips, denoted by "h", from 2 to 10 mm.

the sheath edge[9]. Therefore spatial distribution of the dust cloud would be a rough standard to show the sheath. Each tip was surrounded by each sheath separated through the plasma and dust cloud, which was clearly shown in the pictures. Here the tips were regarded to work for measuring ion density and electron temperature in the dusty plasma.

Figure 5 shows electric characteristics of the circuit for the double-probe method, probe current (I_p) plotted as a function of probe voltage (V_p), with variation of tip height from the bottom electrode in a plasma generated at 40 Pa of Ar and 400 mW of rf power. Ion currents linearly increasing with biasing were observed in regimes of highly negative and positive voltage, denoted by I_{i-} and I_{i+}, respectively. The lines of ion current define parameters of slops, S_{i-} and S_{i+}, and cross-sections on $V_p = 0$, I_{isat-} and I_{isat+} as ion saturation currents. The ion saturation currents tended to increase with tip closing to center of the plasma. The slop of ion current is redefined to be $S \approx S_{i-} \approx S_{i+}$. The linear part around $V_p = 0$ indicates a current from the tip mainly correcting electrons, whose slope, $\frac{dI_p}{dV_p}\Big|_{V_p=0}$, is integrated by an electron energy distribution function in a plasma. It is noted that the slope is enhanced by that of ion current coming from the sheath expanding with biasing tips. Hence electron temperature, T_e is expressed by the formula with following the manner

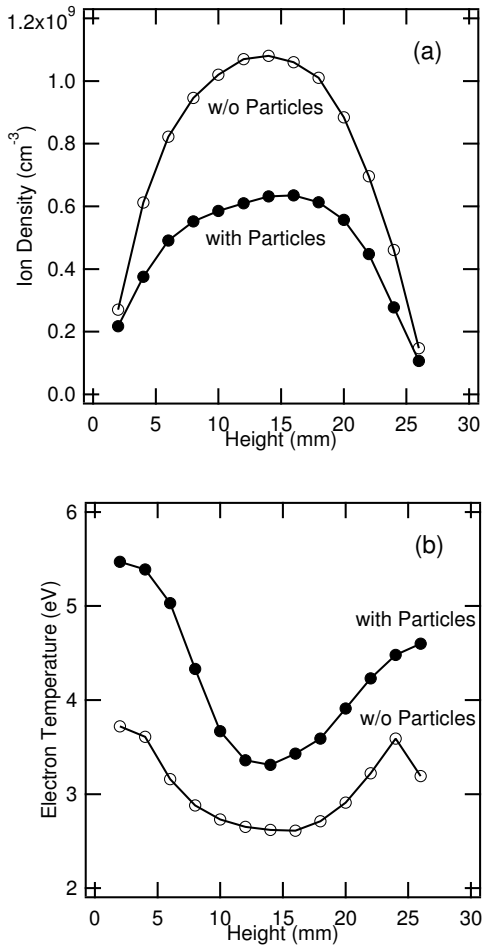

Fig. 6 Spatial distribution profiles of (a) ion density and (b) electron temperature measured by using the double-probe method in the Ar plasma at 40 Pa and 400 mW. Open and solid circles indicate parameters in case without and with the dust particles, respectively.

which suppresses the slope of ion current from that of electron current [10],

$$T_{\mathrm{e}} = \frac{e}{k_{\mathrm{B}}} \frac{|I_{\mathrm{isat-}}| + |I_{\mathrm{isat+}}|}{4\left(\left.\frac{\mathrm{d}I_{\mathrm{p}}}{\mathrm{d}V_{\mathrm{p}}}\right|_{V_{\mathrm{p}}=0} - 0.82S\right)}, \tag{1}$$

where e and k_{B} are elementary charge and the Boltzmann constant, respectively. Ion density, n_{i}, is calculated from the equation,

$$|I_{\mathrm{isat-}}| \approx |I_{\mathrm{isat+}}| = 0.61 n_{\mathrm{i}} e \sqrt{\frac{k_{\mathrm{B}} T_{\mathrm{e}}}{m_{\mathrm{i}}}} A, \tag{2}$$

where m_{i} and A correspond to mass of ion and surface area of the tip, respectively.

3. State of dusty plasmas

Figures 6 (a) and (b) show ion densities and electron temperatures, respectively, measured by using the double-probe method in the Ar plasma at 40 Pa and 400 mW. The spatial distribution profile of ion density around the center should be identical to that of electron density. This profile corresponds to that of pristine plasma derived by the PIC/MCC code. The electron densities expected from the ion densities measured by the double-probe method are higher than those by the hairpin resonator. Therefore it is concluded that the hairpin resonator can affect ionization in volume of the chamber and extinguish the plasma, resulting in reducing electron density and making its spatial profile with two peaks.

In is noted that electron temperature is enhanced throughout the plasma by injecting the dust particles. Density of the dust particle was hard to be precisely measured due to the instability, however, might be reached to 10^6 cm^{-3}. The total area on surface of the dust particle in the cloud can be a few tens mm^2. The plasma should be lost on the surface by recombination between electrons and ions as seen in the measurement of the hairpin resonator. Hence ionization rate should be kept to sustain the plasma, encountering loss by the recombination. This leads to the electron temperature enhanced [11,12]. In Fig. 4, too many dust particles were injected just before extinguishing the plasma. The ion densities in case without the dust particles could not be maintained, although the electron temperature was enhanced (Fig. 6 (a)).

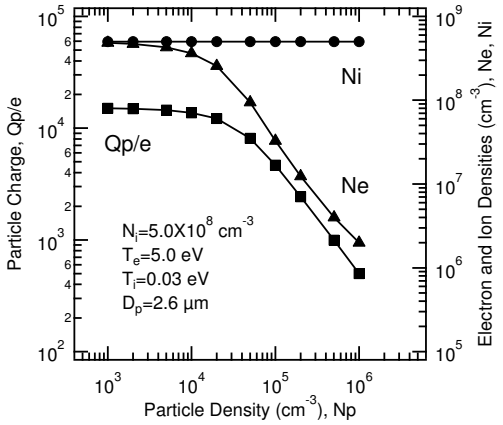

Fig. 7 Variations of electron density and charge of the dust particle calculated from the parameters obtained by the double-probe method in changing dust particle density, and plotted with ion density.

Two parameters of ion density and electron temperature enable to calculate other parameters in dusty plasmas. Electron density and charge of the dust particle are calculated in the orbit-motion-limited (OML) theory[13]. In Fig. 7, assuming the parameters of 5.0×10^8 cm^{-3} for ion density, 5.0 eV for electron temperature, and room temperature for ion temperature, one can estimate the charge of the dust particles to be 10^2–10^4 with varying density of the dust particle. The electron densities should be conserved by charge neutrality in plasmas.

4. Conclusion

The double-probe method seemed to be more appropriate for diagnostics in PK-3 plus than the hairpin resonator. The spatial distribution profiles of ion density obtained by the double-probe method was reasonable compared with the result from the PIC/MCC code. In the PK-3 plus, the electron and ion densities could reached to 10^9 cm^{-3} at several Watts of rf power. Injecting the dust particles, the electron temperature should be enhanced. This may lead to complicate prediction for critical phenomena. The double-probe method, however, gives several measures in ion density and electron temperature for analyzing the phenomena with helps of other theories, e.g., OML.

Acknowledgements

The authors would like to thank members of the PK-3 plus scientific team. This work was supported by the ISS Science Project Office of JAXA. One of the authors (K.T.) thanks Prof. Noriyoshi Sato (Prof. Emeritus Tohoku University) and Prof. Yukio Watanabe (Prof. Emeritus Kyushu University) for valuable discussion.

References

1) Thomas, H. M., Morfill, G. E., Fortov, V. E. *et al.*, New J. Phys., Vol. 10, (2008), 033036.
2) Totsuji, H., J. Phys. A: Math. Theor., Vol. 42, (2009), 214022.
3) Takahashi, K., Hayashi, Y., and Adachi, S., J. Appl. Phys., Vol. 110, (2011), 013307.
4) Heidemann, R., Takahashi, K., Chaudhur, M. *et al.*, unpublished.
5) Johnson, E. O. and Malter, L., Phys. Rev., Vol. 76, (1949), pp. 1411–1412.
6) Johnson, E. O. and Malter, L., Phys. Rev., Vol. 80, (1950), pp. 58–68.
7) Klindworth, M., Piel, A., Melzer, A., Konopka, U., Rothermel, H., Tarantik, K., and Morfill, G. E., Phys. Rev. Lett., Vol. 93, (2004), 195002.
8) Thomas, E., Jr., Avinash, K., and Merlino, R. L., Phys. Plasmas, Vol. 11, (2004), pp. 1770–1774.
9) Barnes, M. S., Keller, J. H., Forster, J. C., O'Neill, J. A., and Coultas, D. K., Phys. Rev. Lett, Vol. 68, (1992), pp. 313–316.
10) Dote, T., Jpn. J. Appl. Phys., Vol. 7, (1968), 964.
11) Carlile, R. N., Geha, S., O'Hanlon, J. J., and Stewart, J., Appl. Phys. Lett., Vol. 59, (1991), pp. 1167–1169.
12) Carlile, R. N. and Geha, S. S., J. Appl. Phys., Vol. 73, (1993), pp. 4785–4793.
13) Mott-Smith, H. M. and Langmuir, I., Phys. Rev., Vol. 28, (1926), pp. 727–763.

Search for Manifestation of Strong Coupling as Critical Point of Fine Particle Plasmas in PK-3 PLUS

Hiroo TOTSUJI [*1], Kazuo TAKAHASHI [*2], and Satoshi ADACHI [*3]

Abstract: The fine particle (dusty) plasma is a charge-neutral mixture of micron-sized fine (dust) particles and ambient plasma composed of ions and electrons. Typical densities of fine particles and ambient plasmas are $(10^4 \sim 10^5)$ cm^{-3} and $(10^6 \sim 10^8)$ cm^{-3}, respectively. Images of fine particles are easily captured and identified by CCD cameras through the scattering of the laser beam and we are able to make particle level observations. In contrast to singly charged ions or electrons, fine particles in plasmas have large negative charges up to 10^3 or even 10^4 times as large as that of an electron, enabling observations of various effects coming from the strong Coulomb coupling between fine particles. For this reason, a lot of researches on fine particle plasmas have been performed recently. One of the most interesting phenomena in strongly coupled systems may be the ones related to the critical point. In this report, we give a summary of our proposal to observe critical phenomena in fine particle plasmas in PK-3PLUS under the condition of the microgravity and the present status of data analysis. In Part I, the theoretical background is given and the possibility to observe the critical point is shown with an emphasis on the difference between the simple one-component plasma (OCP) model of the charged particle systems and systems with the background as real physical entity. In Part II, characteristic parameters realized in PK-3 PLUS are analyzed in relation to those of the critical point. The behavior of the structure factor is discussed in comparison with the effects of inhomogeneity and finiteness of observed samples and conclusions are given.

Keywords: Fine Particle Plasmas, Strong Coupling, Critical Point, PK-3 Plus, Microgravity, ISS

Part I: Theoretical Background

1. One-component plasma (OCP) model

Macroscopic systems of charged particles are usually almost charge neutral including almost the same number of positive and negative charges. In theoretical treatment, however, it is useful to mainly consider only one component. In this case, systems of charged particles are called one-component plasma (OCP). An example of the classical OCP is atomic nuclei in degenerate electrons (the Fermi sea) and that of the degenerate (quantum) OCP is the electron liquid in positively charged jellium. In OCP, the disregarded components which guarantee the charge neutrality of the system are called *background*. It should be noted that, *from the definition of the OCP model, the background has no contribution to physical quantities of the system such as pressure*.

In addition to the neutralization, the background can be considered to be polarizable and, in the case of Debye-Hückel screening, we have the Yukawa OCP. The system of fine (dust) particles in fine particle plasmas (dusty plasmas), charge-neutral mixtures of macroscopic fine particles (dust particles) and ambient plasma of ions and electrons, is one of typical examples for which the Yukawa system is considered to be a model in the first approximation [1–4].

It has been pointed out that fine particle plasmas possibly manifest critical behavior [5–10]. Previously, the existence of the attraction between particles was assumed as the essential requirement for such behavior [5] or the mean field analysis on the Yukawa system was given [6]. Based on the intrinsic tendency of the OCP to become thermodynamically unstable with the increase of the Coulomb coupling [7], we have shown that there appears the critical point when particles are very strongly coupled, taking the deformation of the background plasma explicitly into account [8–10]. Though this condition is not easy to realize in usual experiments, the Yukawa particles in ambient plasma can provide us a possibility of observation of critical behavior at the kinetic level. The only weakness of the system is the effect of the gravity which is inevitable for macroscopic particles necessary for very strong

*1 Okayama University, 3-1-1 Tsushimanaka, Kitaku, Okayama 700-8530, Japan
*2 Department of Electronics, Kyoto Institute of Technology, Matsugasaki, Sakyo-ku, Kyoto 606-8585, Japan
*3 Institute of Space and Astronautical Science, Japan Aerospace Exploration Agency, 2-1-1 Sengen, Tsukuba, Ibaraki 305-8505, Japan
(E-mail: totsuji-09@t.okadai.jp)

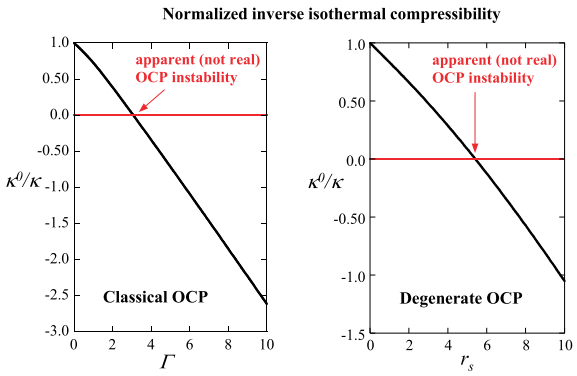

Fig. 1 Inverse isothermal compressibility of one-component plasmas $1/\kappa$ normalized by the ideal gas value $1/\kappa^0$. Classical OCP (left), and degenerate OCP (right). In both cases, the isothermal compressibility has an apparent divergence. In real systems, the contribution of the background should be taken into account.

strong coupling. Therefore fine particle plasmas realized in PK-3 PLUS in the microgravity environment have a possibility to give experimental verification of such phenomena [11].

2. Pressure and isothermal compressibility of OCP

The pressure is given by the volume derivative of the Helmholtz free energy at constant temperature. Within the OCP model, the neutralizing background does not contribute to the pressure of the system: It is assumed to deform automatically *without work* in the process of changing the volume [12].

When the coupling is sufficiently strong, the internal energy of OCP becomes negative due to the negative non-ideal part. The pressure of OCP also becomes negative: This is due to the virial theorem in the case of OCP with pure Coulomb interaction [13] and this occurs also for the Yukawa OCP [8]. Along with the pressure, the inverse isothermal compressibility of the OCP also becomes negative when the coupling becomes strong [8–10,14]. Examples of classical and degenerate pure Coulomb OCP's are shown in Fig. 1 where the coupling in the classical case is expressed by dimensionless parameters $\Gamma = (4\pi n/3)^{1/3} e^2/k_B T$ and, in the degenerate case, by $r_s = (3/4\pi n)^{1/3}/a_B$, n, e, T, and a_B being the number density, the charge, and the temperature and the Bohr radius, respectively.

In contrast to ordinary systems where vanishing of the inverse isothermal compressibility means a thermodynamic instability, vanishing inverse isothermal compressibility does not directly mean such an instability in the case of OCP. In the rigid background, for example, nothing peculiar happens even if the inverse isothermal compressibility of OCP vanishes [14]. The necessity of the background deformation for the observation of the instability has been shown by evaluating the deformation spectrum of the background near the vanishing point of the inverse isothermal compressibility [7].

For real systems, we have to explicitly specify the background. If not completely rigid, the background in systems modeled as OCP has its own pressure which is usually high enough to mask the intrinsic thermodynamic instability of the OCP. In fine particle plasmas, the background plasma is classical and *the Yukawa particles are in polarizing and neutralizing ambient plasma which is deformable in principle*. When the Yukawa particles are sufficiently strongly coupled, their negative contribution to the inverse isothermal compressibility can overcomes the positive contribution from the ambient background plasma. The divergence of the isothermal compressibility of the total system means a thermodynamic instability and density fluctuations are enhanced when we approach to this instability [7]. When the condition of the instability is attained, we may have a transition to a state composed of phases with different densities. We thus expect the existence of the critical point.

3. Yukawa particles in polarizing and neutralizing ambient plasma

Let us consider the system in a volume V composed of N_e electrons with the charge $-e$, N_i ions with the charge e, and N_p particles with the charge $-Qe$, satisfying the charge neutrality

$$(-e)N_e + eN_i + (-Qe)N_p = 0. \tag{1}$$

For densities of electrons, ions, and particles, $n_e = N_e/V$, $n_i = N_i/V$, and $n_p = N_p/V$, we assume n_i, $n_e \gg n_p$ and take the statistical average with respect to electrons and ions to obtain the Helmholtz free energy of the system in the form [15,16]

$$F = F_{id}^{(e)}(T_e, V, N_e) + F_{id}^{(i)}(T_i, V, N_i) + F^{(p)}(T_p, V, N_p), \tag{2}$$

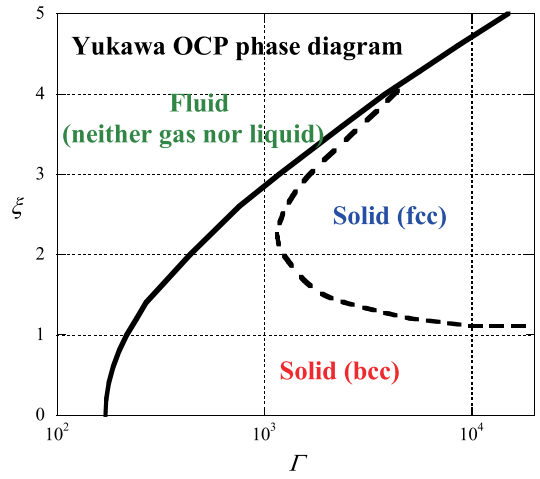

Fig. 2 Phase diagram of Yukawa OCP.

where

$$F^{(p)}(T_p,V,N_p) = -k_B T_p \ln\left[\frac{1}{(2\pi\hbar)^{3N_p}N_p!}\times \iint_V \prod_{i=1}^{N_p} d\mathbf{r}_i d\mathbf{p}_i \exp[-(K_p+U_p)/k_B T_p]\right]. \quad (3)$$

The terms $F_{id}^{(e)}$ and $F_{id}^{(i)}$ are the ideal gas contribution from electrons and ions at temperatures T_e, and T_i, respectively. The term $F^{(p)}$ is the contribution from particles at the temperature T_p where K_p is the kinetic energy of particles and U_p is the Helmholtz free energy for given configuration of particles, $\{\mathbf{r}_i\}_{i=1,2,\ldots N_p}$. We assign different temperatures to particles and ambient microscopic particles.

When we neglect the electron-electron, electron-ion, and ion-ion correlation and regard particles as points, U_p in Eq. (3) is given by a sum of the cohesive energy U_{coh} and the energy associated with the sheath U_{sheath} [15)]

$$U_p = U_{coh} + U_{sheath}, \quad (4)$$

where

$$U_{coh} = \frac{1}{2}\sum_{i\neq j}^{N_p}\frac{(Qe)^2}{r_{ij}}\exp(-r_{ij}/\lambda) - N_p\frac{n_p}{2}\int d\mathbf{r}\frac{(Qe)^2}{r}\exp(-r/\lambda), \quad (5)$$

$$U_{sheath} = -\frac{N_p}{2}\frac{(Qe)^2}{\lambda}, \quad (6)$$

and

$$\frac{1}{\lambda^2} = \frac{4\pi n_e e^2}{k_B T_e} + \frac{4\pi n_i e^2}{k_B T_i}. \quad (7)$$

As indicated by the first term on the right hand side of Eq. (5), the interaction between particles is the repulsive Yukawa potential. Note that, when there is no correlation between particles, $U_{coh} = 0$ due to the second term. Particles develop mutual correlation to reduce U_{coh} to $U_{coh} < 0$ from the uncorrelated value $U_{coh} = 0$. In other words, particles not only interact via the repulsive Yukawa potential but also are *effectively confined* by the second term of Eq. (5) due to the charge neutrality of the whole system [15)]. Though one is tempted to consider that some confining force is necessary to keep repulsive Yukawa particles in a finite volume, charge neutral systems are basically self-confined.

The system of point particles interacting via the Yukawa repulsive potential $(Qe)^2\exp(-r/\lambda)/r$ is called Yukawa one-component plasma (Yukawa OCP) and its static and dynamic properties have been obtained extensively by various methods including numerical simulations [17–19)]. The Yukawa OCP is characterized by the parameters Γ and ξ defined respectively by

$$\Gamma = \frac{(Qe)^2}{ak_B T_p} \quad (8)$$

and

$$\xi = \frac{a}{\lambda}, \quad (9)$$

$a = (3/4\pi n_p)^{1/3}$ being the mean distance between particles. The phase diagram is shown in Fig. 2.

The energy associated with correlation between particles is given by

$$\frac{n_p}{2}\int d\mathbf{r}\frac{(Qe)^2}{r}\exp(-r/\lambda)[g(r)-1], \quad (10)$$

$g(r)$ and $g(r)-1$ being the pair distribution and the pair correlation functions, respectively. We note that this energy (usually called 'internal energy') is nothing but the statistical average of U_{coh}: -1 in [ ] in Eq. (10) corresponds to the subtraction of the second term in U_{coh}.

When $\Gamma \gg 1$, the average values of U_{coh} are well approximated by the Madelung energy of the ground state Yukawa lattice which is either the bcc (for smaller

ξ) or the fcc (for larger ξ) lattice[17–19] with the relative difference of less than 0.01%. We have a simple approximate expression[10]

$$\frac{U_{coh}}{N_p k_B T_p} \approx a_1 \Gamma \exp(a_2 \xi) + a_3 \Gamma^{1/4} \exp(a_4 \xi) \tag{11}$$

with $a_1 = -0.896$, $a_2 = -0.588$, $a_3 = 0.72$, and $a_4 = -0.22$ which reproduces the cohesive energy within relative error less than 1% for $20 \le \Gamma$ and $0 \le \xi \le 5$ (the coefficient $a_1 = -0.896$ is chosen so as to fit both bcc value $-0.89593\ldots$ and fcc value $-0.89587\ldots$ for $\xi = 0$).

We now take the finite size of particles into account, assuming that particles are hard spheres of radius r_p and the charge $-Qe$ is uniformly distributed on the surface. The potential around a particle is given for $r > r_p$, by[20,21]

$$\frac{(-Qe)}{1 + r_p/\lambda} \frac{\exp[-(r - r_p)/\lambda]}{r} = \frac{(-\tilde{Q}e)}{r} \exp(-r/\lambda), \tag{12}$$

where

$$\tilde{Q} = Q \frac{\exp(\tilde{r_p})}{1 + \tilde{r_p}} \tag{13}$$

and

$$\tilde{r_p} = \frac{r_p}{\lambda}. \tag{14}$$

The interaction between particles is then given by the DLVO potential which is still of the Yukawa type out of hard cores

$$\frac{(-\tilde{Q}e)^2}{r} \exp(-r/\lambda) \quad \text{for} \quad r > 2r_p, \tag{15}$$

r being the distance between centers.

In order to express the effect of hard cores of finite radius, we introduce another dimensionless parameter Γ_0 defined by

$$\Gamma_0 = \frac{(Qe)^2}{r_p k_B T_p} = \Gamma \frac{a}{r_p} \tag{16}$$

in addition to Γ and ξ. Values of $\tilde{r}_p$ is related to them as

$$\tilde{r}_p = \frac{r_p}{\lambda} = \frac{a}{\lambda} \frac{r_p}{a} = \xi \frac{\Gamma}{\Gamma_0}. \tag{17}$$

We also define $\tilde{\Gamma}$ by

$$\tilde{\Gamma} = \frac{(\tilde{Q}e)^2}{a k_B T_p} = \Gamma \frac{\exp(2\tilde{r}_p)}{(1 + \tilde{r}_p)^2}. \tag{18}$$

The Yukawa system with hard cores is thus characterized by a set of three dimensionless parameters, (Γ, ξ, Γ_0) or $(\tilde{\Gamma}, \xi, \tilde{r}_p)$. In terms of the latter, the energy associated with the sheath around a particle is written as

$$\frac{\tilde{U}_{sheath}}{N_p k_B T_p} = -\frac{1}{2} \tilde{\Gamma} \xi (1 + \tilde{r}_p) \exp(-2\tilde{r}_p). \tag{19}$$

The Coulombic part of the Helmholtz free energy of the system of particles is then given by

$$\begin{aligned} &\frac{F^{(p)} - F_{id}^{(p)}}{N_p k_B T_p} = f^{(p)}(\tilde{\Gamma}, \xi, \tilde{r}_p) \\ &\approx \int_0^{\tilde{\Gamma}} \frac{d\tilde{\Gamma}}{\tilde{\Gamma}} \frac{\tilde{U}_{coh} + \tilde{U}_{sheath}}{N_p k_B T_p} \\ &= a_1 \tilde{\Gamma} \exp(a_2 \xi) + 4 a_3 \tilde{\Gamma}^{1/4} \exp(a_4 \xi) \\ &+ \frac{3}{2} \tilde{\Gamma} \xi^{-2} [1 - (1 + 2\tilde{r}_p) \exp(-2\tilde{r}_p)] \\ &\quad - \frac{1}{2} \tilde{\Gamma} \xi (1 + \tilde{r}_p) \exp(-2\tilde{r}_p). \end{aligned} \tag{20}$$

For the equation of state given by the hard-sphere part $F_{id}^{(p)}$, we adopt the Carnahan-Stirling formula[22]. From these expressions, we have

$$\begin{aligned} &\frac{p_p}{n_p k_B T_p} \approx \frac{1 + \eta + \eta^2 - \eta^3}{(1 - \eta)^3} \\ &+ a_1 \tilde{\Gamma} e^{a_2 \xi} \left(\frac{1}{3} + \frac{1}{6} a_2 \xi + \frac{\tilde{r}_p^2}{1 + \tilde{r}_p} \right) \\ &+ a_3 \tilde{\Gamma}^{1/4} e^{a_4 \xi} \left(\frac{1}{3} + \frac{2}{3} a_4 \xi + \frac{\tilde{r}_p^2}{1 + \tilde{r}_p} \right) \\ &+ \frac{3}{2} \tilde{\Gamma} \xi^{-2} \frac{\tilde{r}_p^2}{1 + \tilde{r}_p} (1 + e^{-2\tilde{r}_p}) - \frac{1}{4} \tilde{\Gamma} \xi e^{-2\tilde{r}_p} \end{aligned} \tag{21}$$

and the expression for the inverse isothermal compressibility. Here

$$\eta = \left(\frac{r_p}{a} \right)^3 = \left(\frac{\Gamma}{\Gamma_0} \right)^3 \tag{22}$$

is the packing fraction.

The inverse isothermal compressibility can be negative with large absolute values when $\tilde{\Gamma} \gg 1$, the energy associated with the sheath (the fifth term) giving a significant contribution. As a property of the Yukawa OCP, the isothermal compressibility thus diverges at some critical value in the range[8,9] $1 < \tilde{\Gamma} < 10$. The analysis of thermodynamic behavior of the system in

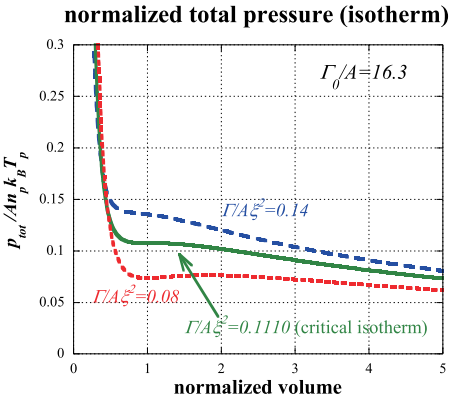

Fig. 3 Examples of the behavior of the total pressure along isotherms.

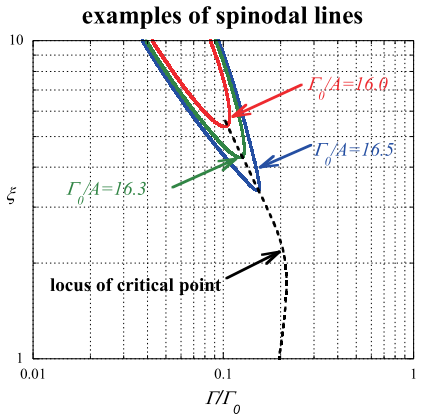

Fig. 4 Spinodal lines and locus of critical point (broken line).

total, however, we have to take the ambient microscopic particles into account whose densities are much larger than particles. Therefore, as is shown below, the effect of diverging compressibility of the Yukawa OCP appears as a property of total system only when $\tilde{\Gamma} \gg 1$ where our interpolation has sufficient accuracy.

Including the contribution of microscopic particles, we have the total pressure of the system p_{tot} approximately expressed as

$$\frac{p_{tot}}{n_p k_B T_p} \approx \frac{A}{1-\eta} + \frac{p_p}{n_p k_B T_p}. \tag{23}$$

Here

$$A = \frac{N_e k_B T_e + N_i k_B T_i}{N_p k_B T_p} \gg 1 \tag{24}$$

is the ratio of ideal gas contribution of microscopic particles to that of particles: The inequality comes from the assumption that the number densities of microscopic particles are much larger than macroscopic particles. We have taken the effect of the finite volume of particles as the reduction of free volume for microscopic particles in the form of the denominator of the first term of Eq. (23). The inverse isothermal compressibility of the system is thus given by

$$\begin{aligned} &-\frac{V}{n_p k_B T_p}\left(\frac{\partial p_{tot}}{\partial V}\right)_{T_e,T_i,T_p} \\ &\approx \frac{A}{(1-\eta)^2} - \frac{V}{n_p k_B T_p}\left(\frac{\partial p_p}{\partial V}\right)_{T_e,T_i,T_p}. \end{aligned} \tag{25}$$

For the thermodynamic instability of our system, the negative contribution to the inverse isothermal compressibility from strongly coupled particles has to overcome not only their own ideal gas contribution but also much larger positive contribution of background plasma. Therefore it is necessary to analyze the instability of the whole system and the background plasma plays an essential role in determining characteristic parameters for such a instability.

4. Thermodynamic instability and phase diagrams

Normalized total pressure of the system $p_{tot}/n_p k_B T_p$ is a function of parameters A, Γ, ξ, and Γ_0. Since usually $A \gg 1$, we have to be at least in the domain $\Gamma_0 > \Gamma \geq A \gg 1$ for the instability and Yukawa particles have to be very strongly coupled. When $\Gamma \gg 1$, $(p_{tot}/n_p k_B T_p)/A$ and $[-V(\partial p_{tot}/\partial V)_T/n_p k_B T_p]/A$, are approximately expressed as functions of $(\Gamma/A,\ \xi,\ \Gamma_0/A)$. Examples of p_{tot}-V isotherms are shown in Fig. 3. Some examples of the lines corresponding to the condition $(\partial p_{tot}/\partial V)_T/n_p k_B T_p = 0$ (spinodal lines) are shown in Fig. 4. The coexisting phases with the common pressure are determined by the usual Maxwell's rule[23]. Examples of resultant phase diagrams in the $(\Gamma,\ \xi)$-plane are shown in Fig. 5. The isotherm corresponds to lines $\xi \propto \Gamma^{1/2}$ in this plane and we have coexisting phases with different densities in the domain inside of phase separation lines. The phase diagrams expressed in terms of another set of variables, $(p_{tot},\ \Gamma/\xi^2)$, are shown in Fig. 6: This is the equivalent of the p-T diagram in the usual gas-liquid phase transition. The line giving coexisting phases ends at the critical point corresponding to the appearance of the extremum in the isotherms or the divergence in the isothermal compressibility. We have enhanced density fluctuations near the critical point[7,8].

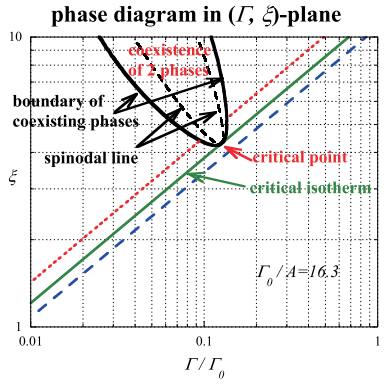

Fig. 5 An example of phase diagram. Inside the solid line, we have a phase separation and the broken line is the spinodal line.

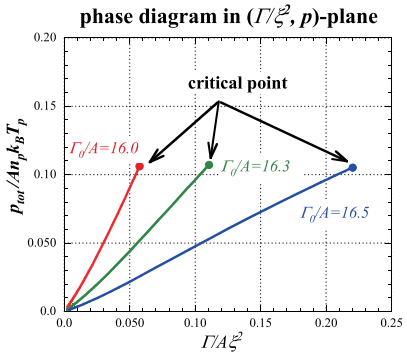

Fig. 6 Phase diagrams and critical points in $(p_{tot}, \Gamma/\xi^2)$-plane.

5. Density fluctuations

The density fluctuation spectrum is related to the dielectric response function via the fluctuation-dissipation theorem. On the other hand, at long wavelengths, the system responds to the perturbation by the compresibility. These relations (the compressibility sum rule) give the density fluctuation spectrum [10)]

$$S(k) \sim \left[-\frac{V}{n_p k_B T_p} \left(\frac{\partial p_{tot}}{\partial V} \right)_{T_i, T_e, T_p} + \mathscr{O}\left(k^2\right) \right]^{-1} \tag{26}$$

indicating the critical behavior of density fluctuations.

For OCP, on the other hand, the fluctuation-dissipation theorem gives the long-wavelength behavior of the structure factor in the form

$$S_{OCP}(k) \sim \left[k_D^2 \lambda^2 - \frac{V}{n_p k_B T_p} \left(\frac{\partial p_p}{\partial V} \right)_{T_p} + \mathscr{O}\left(k^2\right) \right]^{-1}, \tag{27}$$

where $k_D^2 = 4\pi n_p (Qe)^2 / k_B T_p$. (The pressure and the isothermal compressibility here are those of Yukawa OCP.) The vanishing of the inverse isothermal compressibility is not directly related to the enhancement of the density fluctuation. This relation has been derived for OCP's in a polarizing background and confirmed by a comparison with numerical simulations [24)]. In the case of $\lambda \to \infty$ (Coulombic OCP), we have the known result

$$S_{OCP}(k) \sim \left(\frac{k}{k_D} \right)^2 \left[1 - \frac{V}{n_p k_B T_p} \left(\frac{\partial p_p}{\partial V} \right)_{T_p} \left(\frac{k}{k_D} \right)^2 \right]^{-1}. \tag{28}$$

Part II: Experiments

6. Apparatus and experimental parameters

Experiments have been performed in the apparatus PK-3 PLUS, a plasma chamber filled with Ar gas and excited by the rf of 13.56 MHz through the parallel-plate-type electrodes [11)]. Fine particles of several diameters can be injected to the plasma. The diameters, the range of the pressure, and rf power are listed in table 1.

The images of fine particles are scanned by the CCD camera and converted into digital data of coordinates of particles. The velocity of particles is small enough, in comparison with the scanning speed, to give three-dimensional data. The number density of particles is obtained directly.

As for other physical parameters, values are not more than those expected under similar conditions. When one is interested only in the behavior of fine particles, the results of observations are clear. When one tries to relate them to theoretical predictions, however,

Table 1 Parameters in PK-3 Plus.

diameter of fine particles	1.55, 2.55, 3.42 μm
	6.81, 9.19, 14.92 μm
neutral gas	Ar, Ne
neutral gas pressure	5-255 Pa
rf power	0-4000 mW

Table 2 Assumed values of plasma parameters which are not directly measured.

ion density	$(1-10)\cdot 10^8 \mathrm{cm}^{-3}$
ion temperature	300 K
electron density	charge neutrality
electron temperature	(1-3) eV

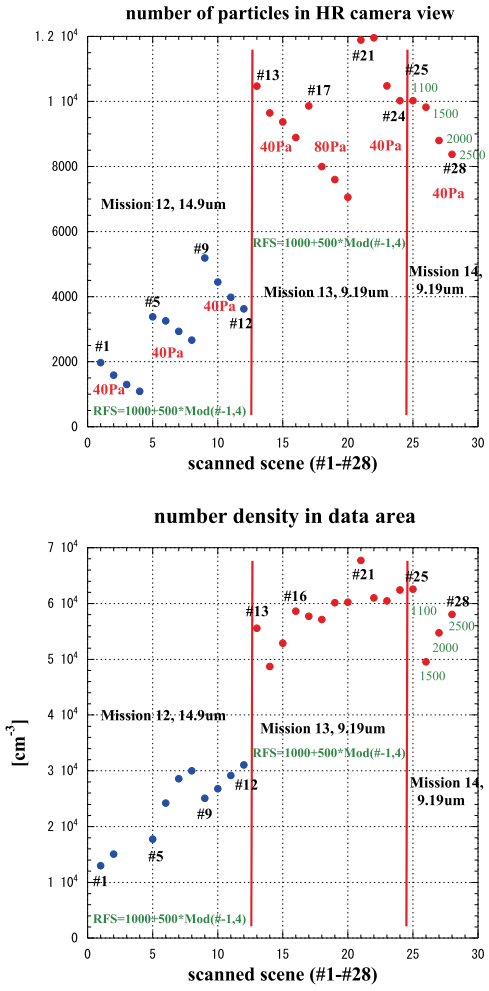

Fig. 7 Parameters of ISS experiments. The number of particles captured by the high resolution (HR) camera and the number density in the domain adopted for observation.

physical parameters not measured directly sometimes become important. In our case, physical parameters of the ambient plasma are mostly nothing more than those extrapolated from similar experiments. They are the electron density n_e, the ion density n_i, the electron temperature T_e, and the ion temperature T_i. We assume them as in Table 2.

To observe the critical point, strongly coupled states of fine particles are necessary. Since the parameter Γ is proportional to the square of the charge of particles, we need high density and high charges of particles. Such a state may be realized by frequent injections of larger particles and high power of rf excitations: Charges on a particle is approximately proportional to the radius and the electron temperature. Parameters for the apparatus, however, have not been well-established for these high density states and trials and errors have been inevitable. From Mission 11 to Mission 14, some sequences of experiments were assigned for our purpose.

In Fig. 7, we plot the number of particles captured by the CCD camera and the number density of particles in samples as function of the "scene" number or the serial number of samples. We observe that, the number and the number density increase with the of scene number. The dependence on the radius of particles has two aspects: Larger particles can have larger charges but also requires high rf excitation which induces larger void.

In order to compare the results with theoretical predictions, the characteristic parameters of experiments are plotted in the $\Gamma/\Gamma_0 - \xi$-plane as shown in Fig. 8. (A preliminary report has been given[25].) Here, contours express the enhancement factor of the density fluctuations and the values of Γ/Γ_0 are directly obtained from the data of experiments. Those of $\xi = a/\lambda$, however, needs the ion density and ion temperature: The electron temperature is believed to be much higher than that of ions and λ is mostly determined by ions. Even if we assume that the ions are at the room temperature, the accurate information of the ion density is lacking and we have to assume that the ion density is $10^8 \sim 10^9$ cm^{-3}. The data points thus vertically move dependent on the ion density.

We observe that the characteristic parameters of experiments are approaching to expected critical point in later Missions. At the same time, we have to admit that they are still far from the target.

7. Structure factor

Let us remember some definitions and relations including the structure factor. The pair correlation function $g(r)-1$ is related to the structure factor $S(k)$ via

$$[g(\mathbf{r})-1] = \frac{1}{(2\pi)^3 n}\int d\mathbf{k}\exp(i\mathbf{k}\cdot\mathbf{r})[S(\mathbf{k})-1] \quad (29)$$

and

$$S(\mathbf{k})-1 = n\int d\mathbf{r}\exp(-i\mathbf{k}\cdot\mathbf{r})[g(\mathbf{r})-1]. \quad (30)$$

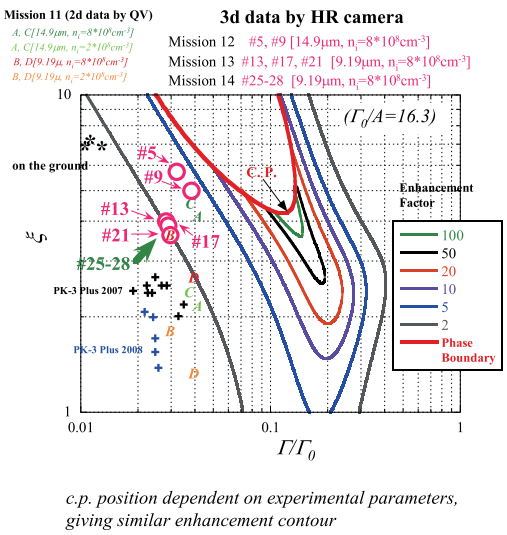

Fig. 8 Characteristic parameters of ISS experiments.

The structure factor is also expressed as

$$S(\mathbf{k}) = \frac{1}{N} < |\rho_{\mathbf{k}}|^2 >, \tag{31}$$

where

$$\rho_{\mathbf{k}} = \sum_{i=1}^{N} \exp(-i\mathbf{k}\cdot\mathbf{r}_i) \tag{32}$$

is called the density fluctuation, N is the total number of particles, and $< >$ denotes the statistical average. Since the computation of $S(\mathbf{k})$ via the Fourier transform of the pair correlation function in the real space does not give reliable result at long wavelengths, we have computed the structure factor directly by Eq. (31).

From three-dimensional distributions of particles, we select the domains as samples which include enough number of particles and, at the same time, are apparently homogeneous. We regard the distribution in the sample is repeated periodically all over the space. We take the average of their squared magnitude over all possible wave numbers within a small range of k, implicitly assuming the spherical symmetry. The size of the sample determines the smallest wave number as the argument of the structure factor.

When the rf power is raised, we have usually the void in the central part of the discharge. Since we have no particles in the domain of void, we have to take our samples from the domain surrounding the void. With the increase of the rf power, the domain of particles' existence becomes thinner and samples, smaller.

An example is shown in Fig. 9. We observe the enhancement of the fluctuation at long wavelengths. In order to confirm that the enhancement near $k = 0$ is not the effect of inhomogeneity, we artificially added such an inhomogeneity to the data of the Yukawa OCP obtained by numerical simulations and compared their effects with our observation. The results are also shown in Fig. 9. We see that, when the density is modified artificially by $\pm 10\%$ within the domain, the structure factor at $k \sim 0$ is enhanced. The extent of enhancement, however, seems to be smaller than what we have observed in experiments: *Though our data may not be*

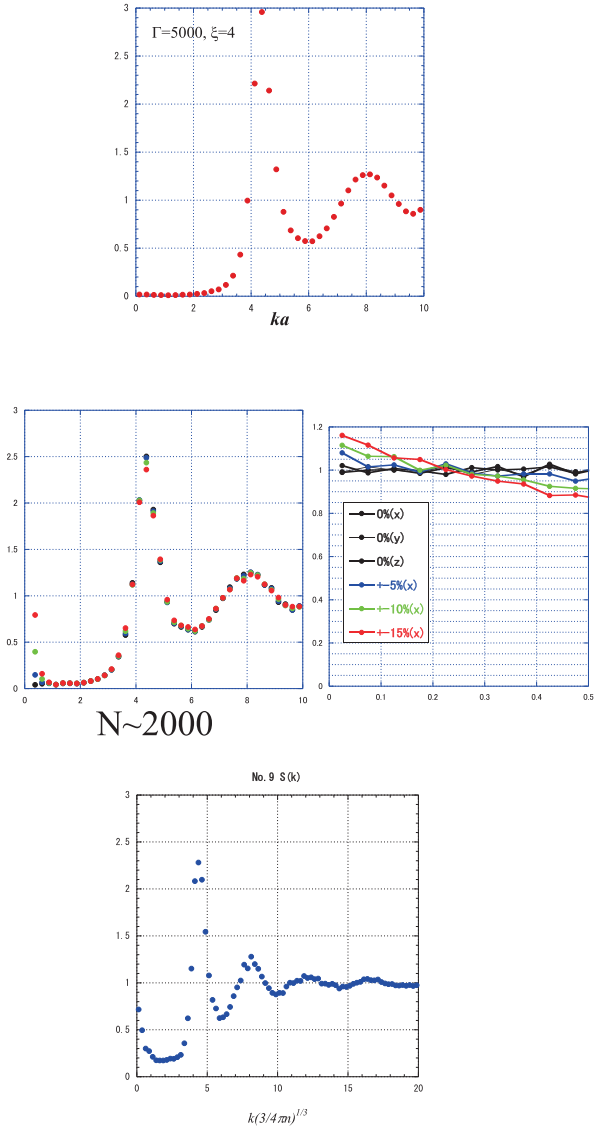

Fig. 9 Effect of artificially-introduced inhomogeneity of the system (middle right), modifying the original structure factor (top) to the one with enhanced fluctuations at long wavelengths (middle left), in comparison with observation (bottom).

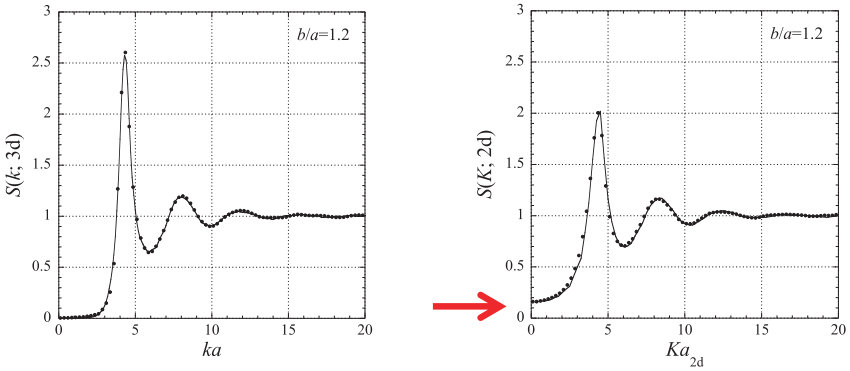

Fig. 10 The enhancement of density fluctuations due to reduction of dimensions (sample size). When three-dimensional sample is sliced into slabs, the original three-dimensional structure factor (left) is observed as the one accompanying the enhanced fluctuations at long but not so long wavelengths (right).

without the effect of inhomogeneity of the system, results obtained by experiments seem to be beyond those effects.

The enhancement of the structure factor in the domain $ka \ll 1$ but not $ka \sim 0$ may attributed to the effect of finiteness of the observed system. In the case where we observe a three-dimensional system through nearly two-dimensional window, we have similar enhancement of the fluctuations[26]. An example is given in Fig. 10. The three-dimensional system is sliced into two-dimensional systems and the three-dimensional coordinates are projected onto a two-dimensional plane. In this process, the fluctuations in the density are enhanced. By the inverse conversion, we are able to recover the original behavior of the structure factor. When we observe a finite domain including large but finite number of particles, we have similar enhancement of fluctuations. We expect to be able to restore the original structure factor which would be observed when we have large enough window. Investigation in this direction is in progress.

8. Conclusions

In order to realize the physical parameters of fine particle plasma corresponding to the possible critical point, high densities with large fine particles are necessary. For high density states, heavy injections and high power of rf excitation are needed. These states have been tried in PK-3 PLUS.

With the increase of the rf power, the void appears in the central part of the plasma. When we have voids, the domain of fine particles is restricted in a relatively narrow region. The domain where particle distribution is homogeneous becomes smaller due to the appearance of voids.

Characteristic parameters have been estimated based on the direct information obtained from observations and also from expectations. Though they have approached to the critical point in the course of experiments, they are still not close to the point.

The structure factor observed in experiments shows the enhancement at long wavelengths. Compared with the effects due to the inhomogeneity of the system which is artificially added, the observed enhancements seem to be larger than expected from those effects. Though we are still not close to the critical point and our data suffer from the effects of inhomogeneity and smallness of samples, the enhancement of the long wavelength fluctuations seems to have been observed. When we are able to have fine particles plasmas without void, closer observations of the critical behavior will be possible.

Acknowledgments

The authors would like to thank members of the research group at Max-Planck Institute for Extraterrestrial Physics lead by Professor G. E. Morfill and the research group at the Joint Institute for High Temperatures lead by Professor V. E. Fortov for kind cooperation throughout this work. They also thank the ISS Science Project Office for financial support.

References

1) Shukla, P. K. and Mamun, A. A., *Introduction to Dusty Plasma Physics*, Inst. Phys., London, 2002.

2) Fortov, V. E., Ivlev, A. V., Khrapak, S. A., Khrapak, A. G., and Morfill, G. E., Phys. Rep., Vol. 421, (2005), pp. 1–103.
3) Tsytovich, V. N., Morfill, G. E., Vladimirov, S. V., and Thomas, H., *Elementary Physics of Complex Plasmas*, Springer, Berlin, 2008.
4) Morfill, G. E. and Ivlev, A. V., Rev. Mod. Phys., Vol. 81, (2009), pp. 1353–1404.
5) Khrapak, S, Morfill, G. E., Ivlev, A. V., Thomas, H. M., Beysens, D. A., Zappoli, B., Fortov, V. E., Lipaev, A. M., and Molotkov, V. I., Phys. Rev. Lett., Vol. 98, (2007), 095003.
6) Avinash, K., Phys. Rev. Lett., Vol. 96, (2006), 015001.
7) Totsuji, H. and Ichimaru, S., Prog. Theor. Phys. Kyoto, Vol. 52, (1974), pp. 42–53.
8) H. Totsuji, Totsuji, H., J. Phys. A: Math. Gen., Vol. 39, (2006), pp. 4565–4569.
9) Totsuji, H., *Non-Neutral Plasma Physics VI, Workshop on Non-Neutral Plasmas 2006*, ed. Drewsen, M., Uggerhøj, and Knudsen, H., AIP Conf. Proc., Vol. 862 (American Inst. Phys., New York, 2006), pp. 248–256.
10) Totsuji, H., Phys. Plasmas, Vol. 15, (2008), 072111.
11) Thomas, H. M., Morfill, G. E., Fortov, V. E. *et al.*, New J. Phys., Vol. 10, (2008), 033036.
12) For example, Pines, D. and Noziéres, P., *The Theory of Quantum Liquids, Vol. I: Normal Liquids*, W. A. Benjamin, New York, 1966, Chap. 3, p. 161.
13) For example, Landau, L. D. and Lifshitz, E. M., *Statistical Physics, 3rd Edition, Part I*, Pergamon, Oxford, 1988, Sect. 31.
14) For example, Baus, M. and Hansen, J.-P., Phys. Rep., Vol. 59, (1980), pp. 1–94.; March, N. H. and Tosi, M. P., *Coulomb Liquids*, Academic Press, London, 1984, Chap. 4.
15) Hamaguchi, S. and Farouki, R. T., J. Chem. Phys., Vol. 101, (1984), pp. 9876–9884.
16) Rosenfeld, Y., Phys. Rev. E, Vol. 49, (1994), pp. 4425–4429.
17) For example, Robbins, M. O., Kremer, K., and Grest, G. S., J. Chem. Phys., Vol. 88, (1988), pp. 3286–3312, and references therein.
18) Farouki, R. T. and Hamaguchi, S., J. Chem. Phys., Vol. 101, (1994), pp. 9885–9893.
19) Hamaguchi, S, Farouki, R. T., and Dubin, D. H. E., Phys. Rev. E, Vol. 56, (1997), pp. 4671–4682.
20) Deryagin, B. and Landau, L., Acta Phys. -Chim. USSR, Vol. 14, (1941), pp. 633–662.
21) Verwey, E. J. W. and Overbeek, J. Th. G., *Theory of the Stability of Lyophobic Colloids*, Elsevier, New York, 1948.
22) Carnahan, N. F. and Stirling, K. E., J. Chem. Phys., Vol. 51, (1969), pp. 635–636.
23) For example, Landau, L. D. and Lifshitz, E. M., *Statistical Physics, 3rd Edition, Part I*, Pergamon, Oxford, 1988, Sect. 84.
24) Totsuji, H. and Tokami, K., Phys. Rev. A, Vol. 30, (1984), pp. 3175–3182.
25) Totsuji, H., Takahashi, K., Adachi, S., Hayashi, Y., and Takayanagi, M., J. Jpn. Soc. Microgravity Appl., Vol. 28, (2011), pp. S27–S30.
26) Totsuji, H, J. Phys. Soc. Jpn., Vol. 78, (2009), 065004; Totsuji, H., J. Phys. Soc. Jpn., Vol. 79, (2010), 064002; Totsuji, H. and Totsuji, C., Phys. Rev. E, Vol. 85, (2012), 031139.